

## ABSTRACT

Knee braces have been increasing in popularity as a means to support joint stability and promote the healing process. In order to enhance the fit, comfort, and design of knee braces, this study investigates knee shape deformations across four knee bending angles from 0 to 90°. Using 3D scanning technology, the knee contours of 50 Asian males aged between 22 and 33 were examined. The reliability of the 3D measurements was validated through comparisons with tape measurements on the actual body. The analysis revealed a stretch of the skin covering the patella bone with a notable vertical strain of 19% and horizontal stretching of 7%. The circumference along the muscle belly at the thigh (15cm above the centre of the patella) and at the calf (7.5cm below the centre of the patella) showed no significant changes with different bending angles, and can be used as an indicator for sizing of knee braces. However, at the patella bone level, the bending of the knee from 0 to 90° increased the knee circumference by 6.4%. The results from sectional analysis showed the asymmetry and the lateral shifting of the knee joint during bending. The findings offer guidelines for the design and optimization of knee braces to address knee deformations and individual body shape variations.

### Keywords

Knee geometry, Gait assessment, Measurement, Optimization methods, Body scanning

## Introduction

The knee, a pivotal joint in the human body, comprises two primary components: the tibiofemoral joint, situated between the tibia and the femur, and the patellofemoral joint, located between the femur and the patella bone. The knee joint is the most complex joint on the human body, facilitating four distinct types of movements: extension, flexion, lateral rotation, and medial rotation [1]. Figure 1 illustrates the knee joint's components at full extension and bending positions, showcasing significant variations in shape and skin strain during bending motions. Given its complexity, the knee is particularly susceptible to injury, especially with advancing age or participation in strenuous physical activities. Common injuries include dislocations and fractures, which elevate the risk of subsequent joint degeneration, such as osteoarthritis. This condition involves the deterioration of joint cartilage and underlying bones, leading to stiffness and a reduced range of motion [2]. Knee injuries also often result in complications, notably instability, [3] where the knee struggles to support the body effectively, causing it to give way, thus impeding routine movements and activities. [4] The prevalence of osteoarthritis in younger individuals is frequently linked to prior knee injuries, driving demand for knee protection and support devices.

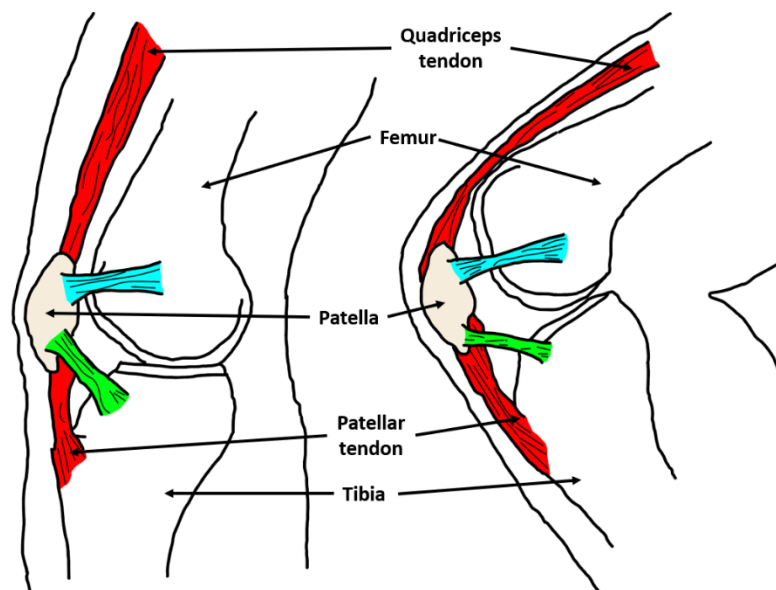


*Figure 1 Composition of knee joint at two different postures*

Knee braces are increasingly prescribed as preventative devices to avoid injuries or aid in recovery by alleviating knee impacts. [5] Typically comprising elastic knitted fabrics as the main body, with foam or elastomeric cushioning parts and/or rigid hinges for support and stabilization, knee braces relieve joint pressure and induce compression, enhancing joint awareness and ensuring secure movement. [6] Consequently, knee braces have become common among athletes, the elderly, and individuals with knee issues or those seeking injury prevention. However, challenges related to fit and comfort often limit their effectiveness and compliance. [7] Slippage, a common discomfort source, is influenced by differences in skin and knee brace deformation. [8] Added et al. [9] found that both hole and non-hole patterns show significant results in helping to relieve pain and improve mobility, with the latter being slightly better overall.

However, determining the optimal knee brace configuration remains challenging due to a lack of consideration for geometric leg and knee parameters, particularly during motion.

Previous studies on knee anthropometric measurements have predominantly focused on assessing the shape of the patella, along with the lengths of the femur and tibia. These evaluations serve various orthopaedic purposes, including preoperative morphological assessments, intraoperative tissue repair, and reconstruction of substantial bone defects. [10] Techniques such as computerized tomography (CT) or three-dimensional (3D) CT have been utilized to provide precise anatomical insights into the body. [11] However, there is a scarcity of studies examining knee geometry variation and skin deformation during motion, particularly concerning wear comfort and anti-slippage properties of knee braces.

To bridge this knowledge gap, this study investigates the dynamics of knee deformation during motion. Employing a 3D body scanning device, comprehensive data on knee morphology and skin strain dynamics are captured. The use of 3D scanning methods for body measurements has been widely studied and adopted. [12, 13] Compared to traditional anthropometric methods involving measurement tape and callipers, 3D scanned image analysis offers several advantages, including efficient measurement of numerous body dimensions and reliable measurements from challenging postures. [14] Choi and Ashdown [15] found that using 3D scanning and image analysis for lower body parts is valuable for apparel design. Additionally, 3D scanned image analysis provides designers with a detailed view of body shape and posture, aiding in the development of orthosis and related products. [16] Additionally, the extensive data collected from 3D scans facilitate the construction of more precise models, contributing to a comprehensive database [17-18]. 3D image analysis serves as a valuable tool for gathering information about the lower limb, aiding in the development of orthosis and related products [19]. Li et al. [20] used whole-body scanning to generate aligned knee data for designing knee braces tailored to military personnel. However, the specific implications drawn from the geometric analysis of the two selected postures were not explicitly stated.

While whole-body scanning is recognized for efficient data acquisition, its high cost and low portability present significant barriers. Handheld scanners offer a cost-effective alternative, especially when precise landmarks are used for data capture. [21] Handheld 3D scanners have been used for studying the hand, foot, and face, and their accuracy has been proven [22,23,24].

In this study, a handheld scanner is utilized to explore knee deformation across four distinct postures, covering a 90° range of motion, representative of daily activities. This exploration aims to identify critical parameters for optimizing knee brace design and enhancing wearer comfort and functionality. The outcomes not only offer guidelines for material selection and knee brace design but also contribute to scientific and academic knowledge by demonstrating a method for extracting key measurements from legs and quantifying knee contours.

## Materials and methods

### Participants

A group of fifty male university students, aged between 22 and 33 years, participated in a 3D knee scanning procedure. Table 1 presents their general information and manually obtained leg and knee measurements in a standing position. Inclusion criteria required participants to be

Asian, healthy, and free from any history of lower limb injury, wounds, visible scars on their knees and lower limbs, or known skin allergies. The experiment received approval from the Human Subjects Ethics Committee of the first author's university and adhered to the principles outlined in the Declaration of Helsinki. Prior to the experiment, participants were provided with an overview, and the experimental procedures were explained to each individual. Written consent was obtained from each participant before commencing the experiment.

TABLE I  
GENERAL INFORMATION OF PARTICIPANTS

	Mean	Min	Max	SD
Age(Years)	26.14	22	33	1.60
Weight(kg)	67.31	48	120	12.68
Height(cm)	173.95	160	198	7.30
BMI	22.15	15.78	30.67	3.07
Circumference of knee (Along the centre of patella)	371.84	315	460	26.22
Circumference of thigh (15 cm from the centre of patella)	471.5	371	613	46.66
Circumference of calf (15 cm from the centre of patella)	367.8	303	433	30.68
Patella vertical length	82.77	62.1	105.63	9.98
Patella horizontal width	80.14	54.31	118.95	13.23

Note: BMI denotes body mass index

## Experiment



*Figure 2 Experimental Procedure Overview*

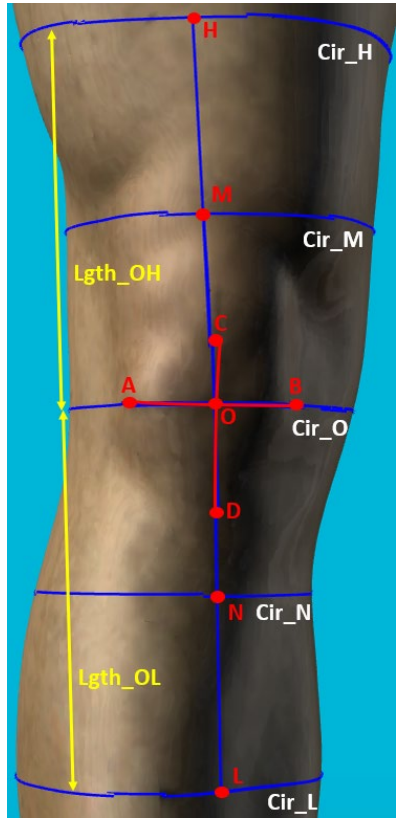
The experiment required participants to perform standing, sitting, and knee-bending tasks at various angles. Each participant's right leg underwent 3D scanning and measurements, consistently conducted by the same technician, as illustrated in Figure 2. The right knee was selected based on the assumption that any observed shape changes would reflect the deformation observed in the left leg.

Initially, participants stood with their feet positioned 50 cm apart. Before initiating 3D scanning, seven landmarks were marked on the leg, and tape measurements were taken in the standing posture. Table 2 summarizes all landmarks positioned on the knee and the measurements taken from their positions in the scan data. The location of the patella was determined through palpation, with five landmarks strategically positioned at the centre of the patella (O) and the midpoints of its four sides (A, B, C, D), forming a cross. Points H and L were situated on the thigh at 15 cm above the centre of the patella along the femur and on the calf 15 cm below the centre of the patella along the tibia, respectively. Circumference measurements were obtained using a measuring tape at the patella's centre (O) and along the thigh (H) and calf (L). These landmarks serve as reliable references on the legs for accurate and repeatable measurements taken on real legs and from 3D scanned images. Palpation and the location of landmarks were performed by the same trained technician for all participants to ensure consistency.

The 3D scanning was performed using a handheld 3D colour scanner (EinScan H, Shining 3D, China), specifically designed for scanning the human body with a hybrid LED and infrared light

source. This scanner featured a built-in colour camera, enabling the construction of 3D meshed data based on texture capture in full colour, providing clear visualization of landmarks. The initial scan was conducted with the right leg straight in a standing position at 0° of bending. Participants were then instructed to sit on a chair and bend their right legs at 30°, 60°, and 90°, while the left legs were kept at 90°. Bending angles were verified using a goniometer before each 3D scanning session, resulting in four 3D scanned images for each participant. The scanning process for each image took approximately 30 seconds, with any slight involuntary movements automatically corrected by the scanning software. Previous research has indicated that the active range of motion (ROM) of the knee joint ranges from 20° to 65°[6], and the complete ROM averages about 132° regardless of age[7]. The examination of ROM from 0° to 90° conducted in this study covers the majority of knee movements encountered in daily activities such as sitting, standing, and walking.

TABLE II  
Landmarks and Measurements

	Item	Description	Illustration
Landmark	O	Centre of patella	
	A	Mid-point of the right side of patella	
	B	Mid-point of the left side of patella	
	C	Mid-point above patella	
	D	Mid-point under patella	
	H	15cm from the centre of patella up to the thigh along the femur	
	L	15cm from the centre of patella down to calf along the tibia	
	M	Mid-point between O and H	
Measurement	N	Mid-point between O and L	
	Cir_O	Circumference at the centre of patella	
	Cir_H	Circumference along H	
	Cir_L	Circumference along L	
	Cir_M	Circumference along M	
	Cir_N	Circumference along N	
	Lgth_OH	Length between O and H on the leg surface	
	Lgth_OL	Length between O and L on the surface of patella	
	Lgth_AB	Length between A and B on the surface of patella	
	Lgth_CD	Length between C and D on the leg surface	
	Ang_Act	Bending angle determined by goniometer	
	Ang_S	Bending angle identified by software	

Knee dimensions obtained from 3D images

The 3D scanned data were imported into a 3D scanning software (M-soft, Techmed 3D, Canada) to extract various dimensions of the knees. The parameters analysed were determined based on the landmarks placed on the knee before the experiment. Additionally, two landmarks, labelled as M and N, were identified from the 3D image with a bending angle of 0°, positioned as the mid-points between O and H, and O and L, respectively.

Using the curve tool available on Msoft, circumferences along the landmarks O, H, L, M, and N were measured. These circumferential dimensions of the legs were evaluated as they are common and important for differentiating sizes of knee braces. Four length measurements were taken along the surface of the leg to assess changes in skin strain during various knee bending activities. Cir\_O, Cir\_H, and Cir\_L were measured from knee images with no bending angle by two different technicians to check inter-operator reliability. The knee bending angle was assessed by placing the goniometer along the joint. The bending angles of the 3D images were measured in the same manner (Figure 3) to ensure alignment and accuracy in the scanned data. While leg dimensions captured in the sitting position may not fully reflect those during movement due to muscle contraction and expansion, this study sheds light on knee variations resulting from bending, an aspect that has not been systematically investigated previously.



Figure 3 Measurement of bending angle from 3D images

Analyses of skin strain and knee shape with different movements

The variations in skin strain on the dimensions, Lgth\_OH, Lgth\_OL, Lgth\_AB (horizontal width of patella) and Lgth\_CD (vertical length of the skin that covers the patella), with different movements were also obtained. The skin strain ( $\epsilon_{skin}$ ) with different bending angles is calculated as:

$$\epsilon_{skin} = \frac{Lgth_{bend} - Lgth_0}{Lgth_0} \times 100\%$$

where  $Lgth_0$  is the length with 0° of bending, and  $Lgth_{bend}$  is the length at different bending angles.

To evaluate the curvature of the skin surface and the lateral displacement of the patella, a sectional view analysis was conducted on the horizontal plane at the O, C, and D levels for all four bending angles. Figure 4a illustrates the sectional view of a knee at the O level. The superimposed sectional views from different bending angles (Figure 4b) enable the observation of knee shape deviations. To achieve alignment of sectional images at different degrees of knee flexion, it is imperative to maintain a standardized positioning and orientation of the knee joint throughout the scanning process across varying bending angle. The front portion of the knee sectional view, which represents the thickness of the patella with skin and tendon, was extracted

for analysis. Measuring the thickness of the patella poses a challenge, even with the use of ultrasonic or Magnetic Resonance Imaging (MRI) devices [25]. The skin thickness, which is typically thin and clinically insignificant, can vary based on factors such as age, sex, and body mass index [26]. Although the patella thickness may also vary due to factors like age, sex, body mass index, and can be influenced by injury, disease, and certain genetic conditions, it is found to be around 2-2.5 cm in adults [27]. Therefore, in the analysis, the thickness of the patella was fixed and assumed to be 3 cm.

As shown in Figure 4c, parameters for quantifying the shape were extracted from the front part of the knee sectional view. A 1 cm distance aligned on the front of the patella was defined as L1. A line parallel to L1, 3cm inward, is defined as L2. The endpoints of L1 on the right and left is marked as P1<sub>R</sub> and P1<sub>L</sub> while the endpoints of L2 on the right and left are marked as P2 and P3, respectively. A perfect arc was formed between P1<sub>R</sub> and P2 and between P1<sub>L</sub> and P3 for comparison with the actual arc in terms of radii, width, height, and length. Each actual arc was divided into four segments to access the deviations from the perfect arc. This analysis can provide insights into the overall shape, curve smoothness, and arc symmetry during various knee movements.

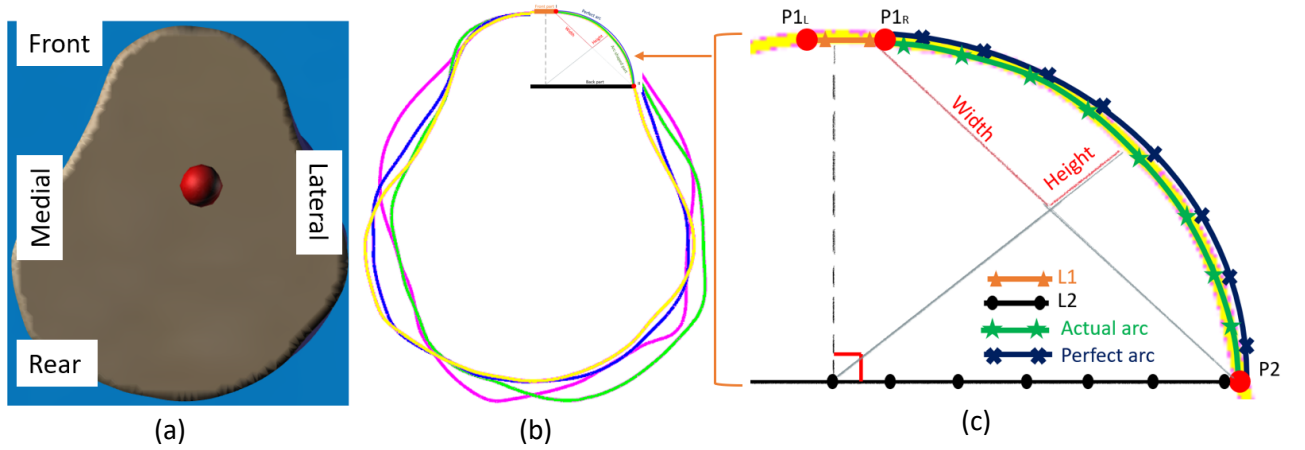


Figure 4 Sectional view of knee obtained at level of Cir\_O from 3D image at 0°, (b) superimposition of sectional views at different bending angles (Purple=90°, Green=60°, Blue=30°, and Yellow=0°) and (c) parameters obtained from the front part of the knee for sectional view analysis

The deviation in curvature was quantified as the difference between the perfect arc delineated between P1 and P2 and the actual arc-shaped of the knee. As shown in Figure 5, the angle perpendicular from the midpoint of L1 to L2 was defined as 90°. The radii at 90° for both actual and perfect arcs were fixed at 3cm (Red bold line in Figure 5). The variation in radii was examined at intervals of every 45° (Interval depicted between thin lines in Figure 5). Analysing the change in radii proves to be a comprehensive method for assessing shape differences, as it directly correlates with the curvature of the knee. Furthermore, adjusting the radii step in high variation areas enables enhanced precision in the analysis. The percentage of deviation (Deviation), which represents the arc shape, was calculated as follows:

$$Deviation = \frac{R_{angle}}{R_{reference}} \times 100\%$$

where  $R_{angle}$  is the radius at specific angles including 0°, 45°, 135°, and 180° and  $R_{reference}$  is the radius at 90°.



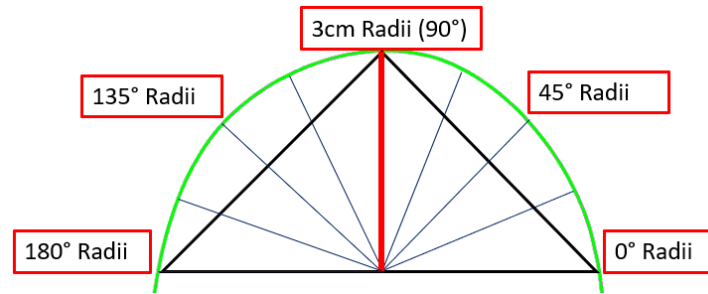


Figure 5 Quantifying Deviation of Knee Curvature from a Perfect Circle using Measured Radii at Various Angles (Red line=Reference line, blue lines=Measured lines)

The side shifting of the patella was calculated to further investigate the asymmetrical shape of the knee. By comparing the centre positions of L1 and L2, the extent of patellar shifting can be determined. Point P4 was defined as the point on L2 perpendicular to the midpoint of L1 whereas L3 was defined as the distance between the P3 and P4. The side shifting (Shift) could then be calculated as

$$Shift = \frac{L2}{2} - L3$$

As shown in Figure 6, a resultant value of 0 indicates precise alignment of the patella within its anatomical boundaries. A negative value signifies lateral deviation of the patella, while a positive value indicates medial deviation.

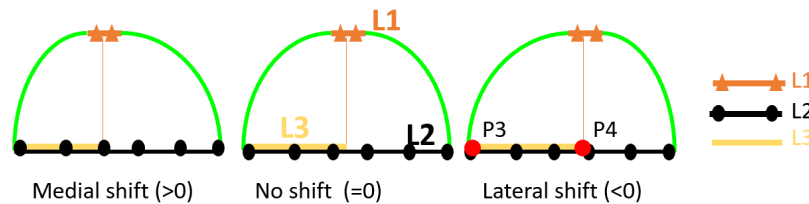


Figure 6 Cases for the assessment of Patellar side shifting in Right Leg

## Statistical analysis

Descriptive statistics, including standard deviation, mean, and coefficient of variation, were calculated for each measurement. The confidence interval was determined using a Student-Fisher coefficient at 95%, taking into account the number of values. Precision was also calculated to ascertain whether sufficient data were collected. The Shapiro-Wilk test was employed to determine if the data followed a normal distribution, given the small sample size (50 individuals) which necessitates a more sensitive test. The null hypothesis for this test assumes that the data follow a normal distribution. The p-values obtained from the test were higher than 0.05, indicating that the null hypothesis could not be rejected and that the data from all measurements are normally distributed. Paired-sample t-tests were performed to compare results from manually obtained measurements and those from the 3D analysis software. Circumferential measurements, Cir\_O, Cir\_H, and Cir\_L, with no bending angle, were compared with those obtained from the 3D images. Inter-operator reliability for obtaining measurements from the 3D images was tested using an intraclass correlation coefficient (ICC). The ICC (2,1) was calculated using a 2-way random effect with single measures and absolute agreement. A repeated measures analysis of variance (ANOVA) was conducted to evaluate the effect of knee bending angles on leg circumference and length measurements. A linear regression model was developed, taking the knee bending angle as the independent variable and skin strain as the dependent variable for Lgth\_OH and Lgth\_OL, to investigate their relationship. Pearson's correlation coefficients were used to examine the relationship between the circumference and length measurements taken at different angles. The significance of using measurements at certain angles to predict the length and skin strain at other angles was assessed through linear regression modelling. The level of significance was set at 0.05.

## Results and discussion

### Reliability of 3D measurements

The ICC (2,1) of the inter-operator reliability on Cir\_O, Cir\_H, and Cir\_L is 0.98 (0.965, 0.989), 0.979 (0.963, 0.988), and 0.995 (0.992, 0.997), respectively. These results indicate that the two technicians can obtain similar circumferential measurement results from the 3D images. The circumferential measurements derived from the 3D images align well with the measurements taken manually with the measurement tape. The measurements obtained from the 3D images by the different technicians exhibit good intra-class correlation, demonstrating the reliability of the 3D analysis.

### Effect of knee bending on circumferential dimensions

Figure 7 depicts the correlation between knee bending angles and leg circumferences for Cir\_H. Repeated measures ANOVA results indicate no significant or predictable changes in Cir\_H and Cir\_N with different bending angles. Cir\_H denotes the circumference along anterior and posterior thigh muscles, deeply situated within the leg and surrounded by other tissues. Muscle contraction or relaxation during knee bending doesn't notably affect the circumference. Similarly, Cir\_N, representing the gastrocnemius muscle belly in the calf region, maintains its circumference unchanged during knee bending, owing to its size and complexity.

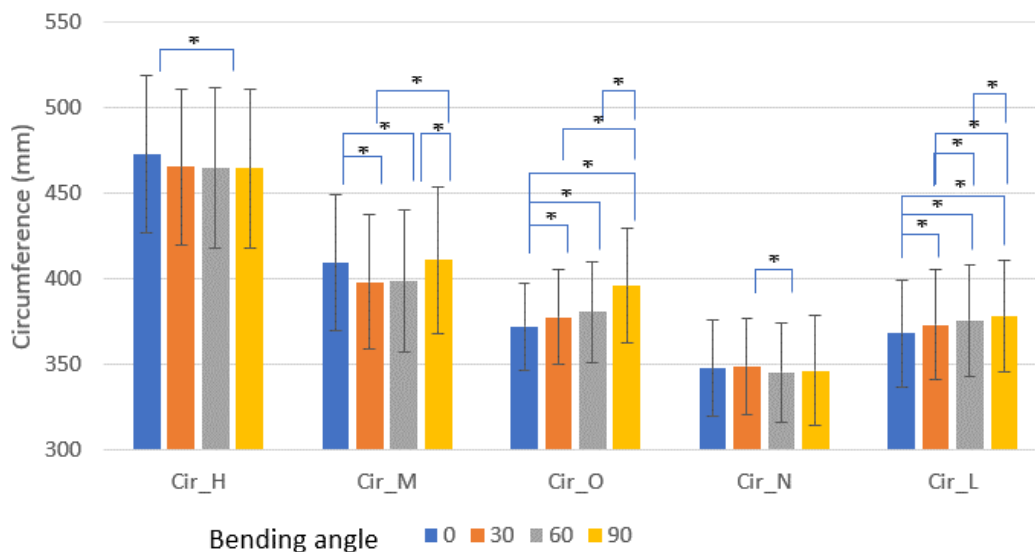


Figure 7 Circumference at different knee bending angles. Error bars indicate  $\pm$  standard deviation and \* indicates significant difference in pairwise comparison ( $p < 0.05$ )

However, the repeated measures ANOVA results revealed significant differences in Cir\_M, Cir\_O, and Cir\_L with changes in knee bending angles. Specifically, Cir\_O, measured at the patella level, exhibited a notable 6.4% increase as the bending angle progressed from 0° to 90°. This increase primarily stemmed from the patella being pushed out from the joint during knee flexion, altering the knee's shape significantly. The patella is a sesamoid bone located within the tendon of the quadriceps muscle and acts as a pulley to enhance muscle leverage. As the knee flexes, the quadriceps muscle pulls on the patella, causing it to protrude from the joint and thereby increasing the circumference.

Cir\_M, measured near the knee cap and muscle attachment points to the knee joint, exhibited non-linear circumference variation during knee bending. This discrepancy could stem from individual morphological factors such as muscle attachment points and bony landmarks affecting the circumference measurement.

Cir\_L represents the measurement taken 15 cm below the patella, focusing on the gastrocnemius muscle that undergoes shape alterations with knee and ankle flexion. The results obtained for Cir\_L were notably clearer compared to other measurements, likely due to this muscle segment being thinner. This thinness likely accentuated circumference changes, distinguishing it from Cir\_N and Cir\_H measurements.

The significant increase in leg circumference at the patella level during knee bending offers crucial insights into knee joint biomechanics. Therefore, greater attention should be directed towards changes in circumference at Landmarks O, M, and L when designing knee braces for optimal support and stability during activities involving knee bending. It's advisable to utilize relatively more elastic materials and a looser fit at these levels to accommodate significant variations during knee bending. Conversely, as variations in Cir\_H and Cir\_N are less pronounced with bending angles, the knee brace ends, requiring more rigidity and tightness to prevent slippage and displacement, should be positioned at H and N levels.

Additionally, Pearson correlation analysis revealed significant correlations ( $p < 0.05$ ) between circumferences measured at different bending angles and measurement's locations, with correlation coefficients ranging from 0.761 to 0.996. This indicates that the circumference of different leg areas can be estimated using a specific circumferential dimension. This suggests that the changes in leg circumference during knee bending are not limited to a particular location or angle but rather exhibit a complex and interconnected relationship. Traditionally, either the circumference at 15 cm above or below the knee midpoint is used to size the knee brace. The results revealed that the circumference at 15 cm above the knee midpoint can serve as a reliable sizing indicator, as it remains independent of posture during measurements. When measuring circumferential dimensions below the knee, it's important to consider the impact of ankle joint plantar flexion.

## Change in skin strain with knee bending angle

### Change in skin strain of the leg

The two leg length measurements, Lgth\_OH and Lgth\_OL, offer insights into variations in skin strain during knee movement. Pierrat et al. [7] suggested that slippage issues stem from problems along the contact surface between knee braces and the skin, emphasizing anatomical considerations in brace design. Therefore, understanding skin strain variations can inform the development of knee braces with reduced slippage or displacement. As illustrated in Figure 8 the increase in Lgth\_OH and Lgth\_OL during knee bending is significant. Compared to the length at the 0° angle, Lgth\_OH increases by 24.8% and Lgth\_OL increases by 20.3% at 90°.

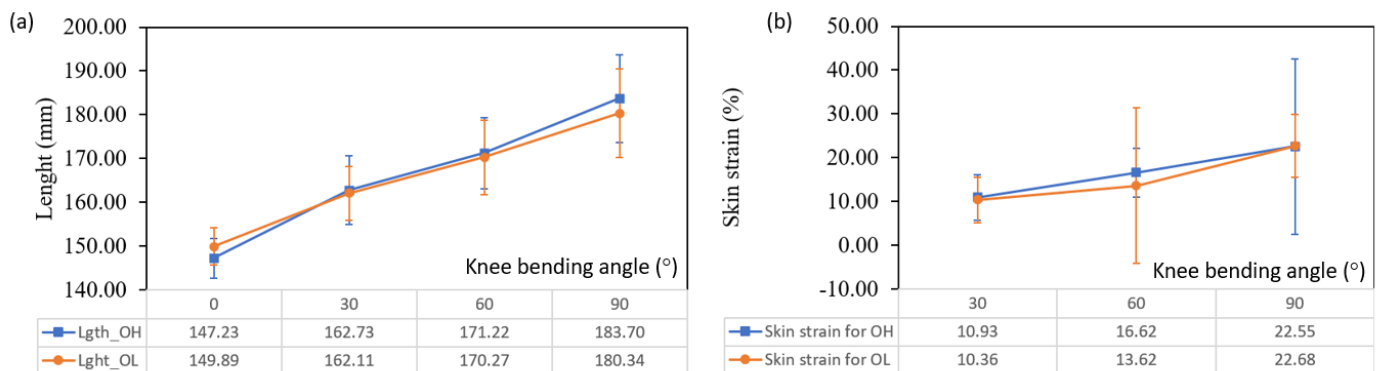


Figure 8 Increase in Lgth\_OH and Lgth\_OL with larger bending angle, and (b) Skin strain at different bending angles

In the study, a fixed distance of 150 mm was utilized at a bending angle of 0°. However, it's important to acknowledge an observed statistical error of approximately 5% in the measured values, despite the fixed distance. This error can be attributed to the inherent distribution of the two lengths, influenced by individual characteristics, as indicated by a coefficient of variation of around 5%. Factors such as slight variations in tape tension, placement errors, and human measurement errors can contribute to differences in tape measurements, leading to a larger standard deviation. In contrast, software-based measurements rely on precise digital techniques, minimizing human errors and providing more consistent and accurate results. A similar pattern was observed for skin strain, with larger variations noted at 60° and 90° angles, corresponding to moments of knee bending when muscles are most solicited. This variability likely stems from individual anthropometric characteristics such as body weight and muscle mass, impacting strain distribution on the skin surface.

A linear regression analysis was conducted to examine the relationship between the bending angle and changes in Lgth\_OH and Lgth\_OL. The results revealed the following equations:  $Lgth\_OH = \text{Bending angle} \times 0.394 + 148.497$  ( $R^2 = 0.739$ ) and  $Lgth\_OL = \text{Bending angle} \times 0.332 + 150.727$  ( $R^2 = 0.683$ ).

Both Lgth\_OH and Lgth\_OL demonstrated a significantly linear relationship with the bending angle. It is also important to know if the length of the knee or amount of skin strain can be estimated from the length at a particular bending angle to design a knee brace that can address knee movement. Pearson's correlation coefficients were calculated for the two length measurements across different bending angles. Among Lgth\_OH measurements, only those taken at 30° showed significant correlation ( $p < 0.05$ ) with measurements at 0° ( $R = 0.35$ ), 60° ( $R = 0.57$ ), and 90° ( $R = 0.76$ ). Conversely, Lgth\_OL at 60° exhibited significant correlation with

measurements at 0° (R = 0.31), 60° (R = 0.68), and 90° (R = 0.69). Table 3 illustrates the linear regression model using Lgth\_OH at 30° and Lgth\_OL at 60° to estimate lengths at other bending angles.

The coefficient of determination (R<sup>2</sup>) for the regression equation to calculate length at 0° is relatively small, with only 0.12 and 0.1 for Lgth\_OH and Lgth\_OL. This indicates that only 12% of Lgth\_OH and 10% of Lgth\_OL at 0° can be explained by Lgth\_OH at 30° and Lgth\_OL at 60°. For the regression equations to calculate length at other bending angles, R<sup>2</sup> moderately ranges from 0.33 to 0.58. This suggests that the regression model could be further optimized by considering additional factors such as other geometrical leg data or even subject morphology. Investigating variables related to a person's physical ability, such as joint flexibility, may offer new insights into refining the regression model and enhancing its predictive capabilities.

TABLE III  
RESULTS OF LINEAR REGRESSION ANALYSIS OF LENGTH MEASUREMENTS

Independent variable (X)	Dependent variable (Y)	Regression equation	R <sup>2</sup>	F	p
	Lgth_OH_0°	Y= X (0.205) + 113.589	<b>0.12</b>	5.97	0.02
<i>Lgth_OH_30°</i>	Lgth_OH_60°	Y= X (0.583) + 76.272	<b>0.33</b>	19.83	0.00
	Lgth_OH_90°	Y= X (0.822) + 50.340	<b>0.58</b>	53.15	0.00
	Lgth_OL_0°	Y= X (0.157) + 123.171	<b>0.10</b>	5.00	0.03
<i>Lgth_OL_60°</i>	Lgth_OL_30°	Y= X (0.482) + 80.3	<b>0.46</b>	40.06	0.00
	Lgth_OL_90°	Y= X (0.816) + 41.694	<b>0.48</b>	42.29	0.00

R<sup>2</sup> denotes the coefficient of determination.

#### Change in skin strain at around the patella

The patella plays a significant role in skin strain changes during leg movement, with many knee braces incorporating a patella hole to accommodate this movement. Figure 9 illustrates the lengths of Lgth\_AB and Lgth\_CD at various bending angles. Results indicate that Lgth\_CD increases by 19% between 0° and 90°, suggesting that most deformations observed in Lgth\_OH and Lgth\_OL stem from the skin covering the patella. Notably, the majority of deformation occurs during movement initiation, particularly between 0° and 30°, where the deformation reaches nearly 12%. Conversely, the change in Lgth\_AB is 7% between 0° and 90°, with less variation compared to Lgth\_CD, boasting an accuracy of 3.8% during the experiment compared to 5.3% for Lgth\_CD. Skin strain change in the leg follows a linear pattern, primarily around the patella during knee bending. This underscores the importance of knee braces addressing patellar deformation to alleviate discomfort and movement burden for wearers.

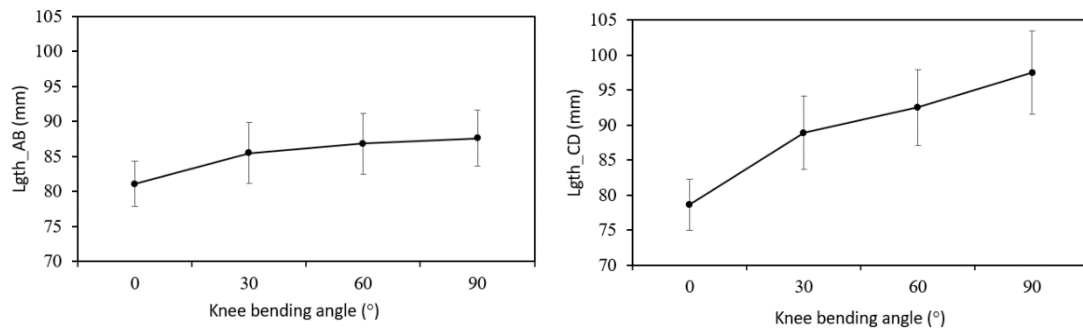


Figure 9 Lengths of (a) Lgth\_AB and (b) Lgth\_CD at different bending angles

As depicted in Figure 10, a knee brace may fit snugly at a standing posture but may form gaps and wrinkles when the knee bends. Utilizing materials like highly elastic knitted fabrics, which are stretchable and flexible, can effectively accommodate changes in knee shape and movement during physical activities. Understanding skin strain levels at different bending angles aids in selecting appropriate elastic materials with suitable tensile properties tailored to specific end-uses and leg movements. These materials should possess enough elasticity to accommodate skin strain during dynamic motions, while also offering sufficient stiffness and stability to prevent knee overstretching and subsequent injuries.

In knee brace design, areas experiencing high skin strain, such as around the patella, may benefit from additional support or padding to prevent injury. Conversely, regions with low skin strain might require less rigid structures, enhancing flexibility and comfort. Knee braces with patella holes allow space for the geometric variation of the patella. Monitoring changes in patella shape and dimensions during bending can inform the sizing of the patella hole and the elasticity required for materials surrounding it in the brace design.



Figure 10 . A commercially available knee brace on knee at standing and bending positions

#### Effect of the morphology of patella

A sectional analysis was conducted to assess differences in curvature across varying bending angles at three distinct horizontal sections of the patella. Figure 11 illustrates the deviations, expressed in radius, from the actual arc to the perfect arc at every 45° interval at levels C, O, and D. From 45° to 135°, the patella curvature closely resembles a perfect circular arc shape,

regardless of the bending angle. The deviations are slightly less than 100%, indicating slightly higher curvatures, at bending angles of 30° and 60° on both 45° and 135° measuring angles of the patella at level O and only at the 45° measuring angle at level D. However, beyond 45° on both the left and right sides from the patella centre, an increase in radius is noticeable, suggesting a relatively flatter patella shape rather than perfect circularity. The deviation in radius significantly highlights patellar asymmetry on the medial and lateral sides of the knee. Compared to the radius of the perfect arc, the radius at 180° (medial side) increased by  $38\% \pm 8\%$ , whereas at 0° (lateral side), it increased by only  $18\% \pm 6\%$ . Given that curvature is calculated as  $1/\text{radius}$ , these findings indicate significantly higher curvature on the lateral side compared to the medial side. At 0° and 180° measuring angles (patellar edges), deviation is notably higher in the horizontal plane at level C compared to levels O and D. This observed asymmetry in knee morphology underscores a non-symmetrical curvature, with pronounced asymmetry at the patellar edge.

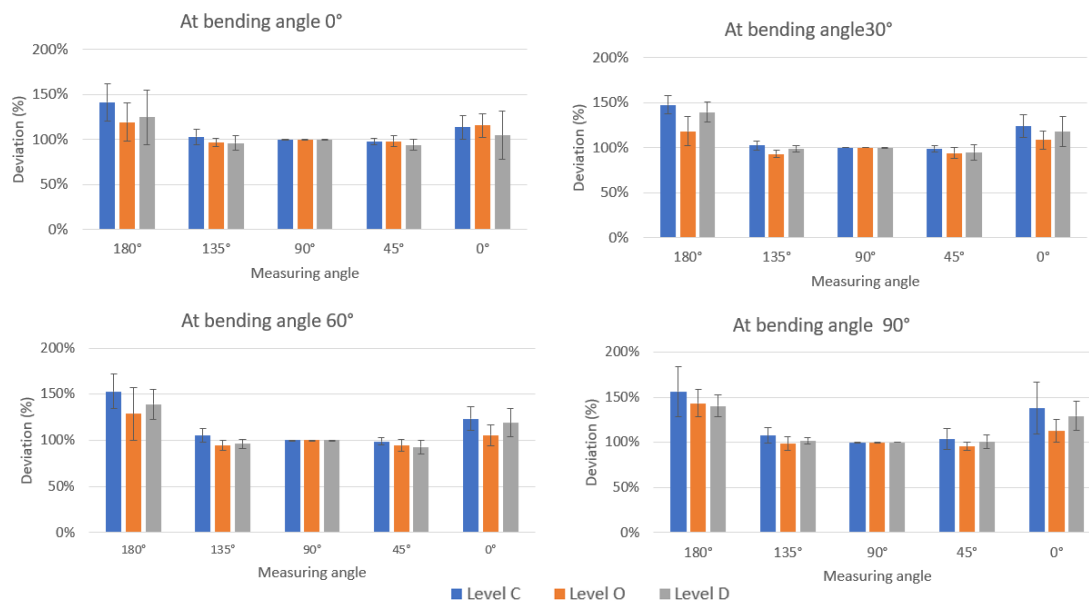


Figure 11 Deviation of knee

The results of the side shifting of the patella at different bending angles and levels are presented in Table IV, showing a relatively high coefficient of variation ranging from 50% to 100%. This suggests that the side shifting of the patella is heavily influenced by individual differences, even among individuals with similarly shaped knee joints. The shift ratio, ranging from -0.1 to -0.5, indicates a significant displacement towards the lateral side, with knee bending from 0 to 90° further accentuating this lateral shift. However, significant differences are noted in the shift ratio between the center and the top and bottom of the patella, confirming the irregular and asymmetric shape of the patella. The observed variability at these levels may stem from individual anatomical differences, variations in muscle activity, or other factors influencing patella position. Moreover, the results underscore that asymmetry is heightened when the knee is bent. This information is invaluable in designing knee braces or other medical devices aimed at providing knee joint support and stability. By identifying the patella as a zone with significant shape deformation, targeted interventions can be supported during the design stage.



TABLE IV  
PATELLA SHIFT

Location	0°	30°	60°	90°
At the Level of Landmark C	$-0.42 \pm 0.19$	$-0.36 \pm 0.16$	$-0.44 \pm 0.22$	$-0.28 \pm 0.40$
At the Level of Landmark O	$-0.05 \pm 0.11$	$-0.15 \pm 0.19$	$-0.35 \pm 0.15$	$-0.46 \pm 0.23$
At the Level of Landmark D	$-0.30 \pm 0.17$	$-0.33 \pm 0.27$	$-0.30 \pm 0.28$	$-0.17 \pm 0.28$

Incorporating the asymmetric position of the patella, particularly during knee flexion, into knee brace design presents opportunities for improvement. One recommendation is to explore the use of flexible and stretchable materials, such as knit fabric, as alternatives to the rigid foam commonly used in traditional knee braces. Utilizing knit fabric could enhance knee brace effectiveness and treatment outcomes by better conforming to the unique shape and movement of individual knees during physical activities. Additionally, the asymmetrical shape of the knee joint has significant implications for the placement of the patella hole in knee braces. Most knee braces with patella holes on the market feature symmetrical designs, which may not offer optimal support and stabilization to the knee joint, especially on the side with the larger curvature. Therefore, adapting knee brace designs to accommodate asymmetry could lead to improved functionality and comfort for users.

A limitation of this study is the restricted participant pool, comprising 50 healthy Asian males aged between 22 and 33 years, without considering weight and height groups. This limitation hampers the statistical generalizability of our findings to a broader population of knee brace users. Therefore, further research on diverse populations is warranted to encompass a wider range of age groups, weight categories, ethnicities, and genders. Incorporating a broader spectrum of parameters beyond knee geometry and body mass index (BMI), such as muscular strength and joint flexibility, could facilitate the development of a more comprehensive model of knee dynamics.

## Conclusion

This study employed 3D scanning and image analysis techniques to assess alterations in knee shape during movement, in order to ensure measurement accuracy, especially for challenging or hard-to-maintain positions. The knee data at bending angles ranging from 0° to 90° was obtained from 50 Asian males aged between 22 and 33 years. The following findings were identified:

- The circumference along the muscle belly at thigh (15cm above the centre of patella) and at calf (7.5cm below the centre of patella) have no significant changes with different bending angles. These measurements can serve as indicators for knee brace sizing.
- Significant variations with the bending angles were found on the circumferences at patella and other levels of thigh and calf
- As the leg bends from a standing straight position to 90°, the skin of the leg significantly stretches, with Lgth\_OH and Lgth\_OL increasing by 24.8% and 20.3% respectively. This extension primarily occurs around the patella, with the vertical length of the patella increasing by 19%. This stretching is most pronounced during the initiation of movement in the vertical direction.

- The sectional view analysis quantifies the asymmetry of the knee and patella through radius measurement from the centre of the patella. The patella exhibits a deviation in terms of radius from a perfect arc by 38% on the medial side and 18% on the lateral side. The deviation at the top level of the patella is 10% greater than that at the bottom and middle levels.
- The patella shifts laterally when bending and the shifting is susceptible to individual differences.

The study outcomes offer valuable insights into the structural properties of the knee joint and have significant implications for the development of more effective treatment strategies for knee injuries and disorders. The data on circumference variation, skin strain changes, asymmetry, and patella shifting can guide the selection of fabrics and materials. Suitable elastic fabric can be incorporated in specific zones of the knee brace, strategically adapting to the biomechanics of the knee to match knee deformation with appropriate fabric tensile properties. The use of a perforated or "holed" design to accommodate the variation at the patella could be a potential strategy for reducing the contact zone, thereby minimizing the risk of slippage during movement. The practical application of these strategies will be further explored in a subsequent study, which aims to design knee braces based on variations in knee brace stretching properties compared to the skin and shape of the patella hole. It is also recommended to expand the subject types to comprehensively summarize knee joint morphology and changes in different populations, providing a reference for designing more personalized knee protectors in clinical settings.

## Reference

1. Pereira S., Anand S., Rajendran S., & Wood C. (2007). *A study of the structure and properties of novel fabrics for knee braces*, Journal of Industrial Textiles, 36(4), 279-300, <https://doi.org/10.1177/1528083707072357>.
2. Siebers H., Eschweiler J., Pinz J., Tingart M., & Rath B. (2020). *The effect of a knee brace in dynamic motion—An instrumented gait analysis*, PLOS ONE, 15(9), <https://doi.org/10.1371/journal.pone.0238722>.
3. King L.K., Kendzerska T., Waugh E.J. & Hawker G.A. (2018). *Impact of Osteoarthritis on Difficulty Walking: A Population-Based Study*, Arthritis Care Res, 70, 71-79, <https://doi.org/10.1002/acr.23250>.
4. Pérez-Soriano P., García-Roig Á., Sanchis-Sanchis R. & Aparicio I. (2019). *Influence of compression sportswear on recovery and performance: A systematic review*, Journal of Industrial Textiles, 8(9), 1505-1524, <https://doi.org/10.1177/1528083718764912>.
5. Beaudreuil J., Bendaya S., Faucher M., Coudeyre E., Ribinik P., Revel M. & Rannou F. (2009). *Clinical practice guidelines for rest orthosis, knee sleeves, and unloading knee braces in knee osteoarthritis*, Joint Bone Spine, 76(6), 629-636, <https://doi.org/10.1016/j.jbspin.2009.02.002>.
6. Styf J. (2012). *The Effects of Functional Knee Bracing on Muscle Function and Performance*, Sports Med, 28, 77–81, <https://doi.org/10.2165/00007256-199928020-00002>.
7. Squyer E., Stamper D.L., Hamilton D.T., Sabin J.A & Leopold S. (2013). *Unloader Knee Braces for Osteoarthritis: Do Patients Actually Wear Them?*, Clin Orthop Relat Res, 471, 1982–1991, <https://doi.org/10.1007/s11999-013-2814-0>.
8. Pierrat B., Millot C., Molimard J., Navarro L., Calmels P., Edouard P. & Avril S. (2015). *Characterisation of Knee Brace Migration and Associated Skin Deformation During Flexion by*

- Full-Field Measurements*, Experimental Mechanics, 55, 349–360, <https://doi.org/10.1007/s11340-014-9947-2>.
9. Added M.A.N., Added C., Kasawara K.T., Rotta P.V. & Diego De Freitas G. (2017) *Effects of a Knee Brace with a Patellar Hole Versus Without a Patellar Hole in Patients with Knee Osteoarthritis: A Double-Blind, Randomized Controlled Trial*, Evaluation & the Health Professions, 41(4), 512-532, <https://doi.org/10.1177/0163278717714307>.
  10. Feng R., Zhong Q., Zheng L., Ye H., Luo D., Ding M., Pang N., Li J. & Yao Y. (2022) *Study on the morphological characteristics and rotational alignment axis of placement plane of the tibial component in total knee arthroplasty for hemophilia-related knee arthritis*, Journal of Orthopaedic Surgery and Research, 17(1), 315, <https://doi.org/10.1186/s13018-022-03176-4>.
  11. Balwan A.R., Shinde V.D. (2020). *Development of patient specific knee joint implant*, Materials Today: Proceedings, 27(1), 288-293, <https://doi.org/10.1016/j.matpr.2019.11.032>.
  12. Han H., Nam Y. & Choi K. (2010) *Comparative analysis of 3D body scan measurements and manual measurements of size Korea adult females*, International Journal of Industrial Ergonomics, 40, 530-540. <https://doi.org/10.1016/j.ergon.2010.06.002>.
  13. Alemany S., Remon A., Ballester A., Durá J.V., Nácher B., Parrilla E. & González J.C. (2022). *Data management and processing of 3D body scans*, Digital Manufacturing Technology for Sustainable Anthropometric Apparel, Woodhead Publishing, 97-116, <https://doi.org/10.1016/B978-0-12-823969-8.00007-1>.
  14. Yu A., Yick K.L. & Wong S.T. (2021). *Analysis of length of finger segments with different hand postures to enhance glove design*, Applied Ergonomics, 94, <https://doi.org/10.1016/j.apergo.2021.103409>.
  15. Choi S. & Ashdown S. (2011). *3D body scan analysis of dimensional change in lower body measurements for active body positions*, Textile Research Journal, 81(1), 81–93, <https://doi.org/10.1177/0040517510377822>.
  16. Kwan, M. Y., Yick, K. L., Chow, L., Yu, A., Ng, S. P., & Yip, J. (2021). *Impact of postural variation on hand measurements: Three-dimensional anatomical analysis*, PLOS ONE, 16(4). <https://doi.org/10.1371/journal.pone.0250428>.
  17. Seminati E., Canepa Talamas D., Young M., Twiste M., Dhokia V., & Bilzon J. L. J. (2017). *Validity and reliability of a novel 3D scanner for assessment of the shape and volume of amputees' residual limb models*, PLOS ONE, 12(9). <https://doi.org/10.1371/journal.pone.0184498>.
  18. Dessery, Y., & Pallari, J. (2018). *Measurements agreement between low-cost and high-level handheld 3D scanners to scan the knee for designing a 3D printed knee brace*, PLOS ONE, 13(1), <https://doi.org/10.1371/journal.pone.0190585>.
  19. Powers O.A., Palmer J.R. & Wilken J.M., (2022), *Reliability and validity of 3D limb scanning for ankle-foot orthosis fitting*, Prosthetics and Orthotics International, 46, <https://doi.org/10.1097/PXR.0000000000000066>.
  20. Li P., Corner B., Hurley M., Powell C. & LaFleur A. (2015). *Three-dimensional (3D) Analysis of Knee Shape for Designing a Knee-pad*, Procedia Manufacturing, 3, 3689 – 3693, <https://doi.org/10.1016/j.promfg.2015.07.790>.
  21. Xia S., Guo S., Li J. & Istook C. (2019). *Comparison of different body measurement techniques: 3D stationary scanner, 3D handheld scanner, and tape measurement*, The Journal of The Textile Institute, 110(8), 1103-1113, <https://doi.org/10.1080/00405000.2018.1541437>.

22. Ma Y., Yang E. & Lin W. (2024). *Using the depth deviation based on three-dimensional images to evaluate the correction of nasolabial folds: A prospective and quantitative analysis*. *Journal of Cosmetic Dermatology*, 23, 607-613, <https://doi.org/10.1111/jocd.16011>.
23. Susanto N., Mahachandra M., Budiawan W, Rizkiyah E. & Apsari C. D. (2023). *Determining optimal lighting in 3D scanner for hand foot static anthropometric measurements*. *Cogent Engineering*, 10, 2233248, <https://doi.org/10.1080/23311916.2023.2233248>.
24. Amornvit P. & Sanohkan S. (2019). *The Accuracy of Digital Face Scans Obtained from 3D Scanners: An In Vitro Study*. *International Journal of Environmental Research and Public Health*, 16(24), 5061, <https://doi.org/10.3390/ijerph16245061>.
25. Nishida Y, Nishino T, Tanaka K, Onishi S, Kanamori A & Yamazaki M. (2021). *An Objective Measure of Patellar Tendon Thickness Based on Ultrasonography and MRI in University Athletes*. *Journal of clinical medicine*, 10(18), 4092, <https://doi.org/10.3390/jcm10184092>.
26. Basso O., Johnson D. P., & Amis A. A. (2001). *The anatomy of the patellar tendon*. *Knee surgery, sports traumatology, arthroscopy: official journal of the ESSKA*, 9(1), 2–5, <https://doi.org/10.1007/s001670000133>.
27. Song S. J., Kang S. G., Park C. H., & Bae D. K. (2018). *Comparison of Clinical Results and Risk of Patellar Injury between Attune and PFC Sigma Knee Systems*. *Knee surgery & related research*, 30(4), 334–340, <https://doi.org/10.5792/ksrr.18.020>.